J|A|C|S
ARTICLES
Published on Web 01/26/2008

Hydrogenation of Single-Wall Carbon Nanotubes Using Polyamine Reagents: Combined Experimental and Theoretical Study

Glen P. Miller,*,† Jeremy Kintigh,† Eunja Kim,‡ Philippe F. Weck,§ Savas Berber,|| and David Tománek*,||

Department of Chemistry and Materials Science Program, University of New Hampshire, Durham, New Hampshire 03824, Department of Physics and Astronomy, University of Nevada Las Vegas, 4505 Maryland Parkway, Las Vegas, Nevada 89154, Department of Chemistry, University of Nevada Las Vegas, 4505 Maryland Parkway, Las Vegas, Nevada 89154, and Physics and Astronomy Department, Michigan State University, East Lansing, Michigan 48824-2320

Received September 30, 2007; E-mail: glen.miller@unh.edu; tomanek@msu.edu

Abstract: We combine experimental observations with *ab initio* calculations to study the reversible hydrogenation of single-wall carbon nanotubes using high boiling polyamines as hydrogenation reagents. Our calculations characterize the nature of the adsorption bond and identify preferential adsorption geometries at different coverages. We find the barrier for sigmatropic rearrangement of chemisorbed hydrogen atoms to be ~1 eV, thus facilitating surface diffusion and formation of energetically favored, axially aligned adsorbate chains. Chemisorbed hydrogen modifies the structure and stability of nanotubes significantly and increases the inter-tube distance, thus explaining the improved dispersability in solvents like methanol, ethanol, chloroform, and benzene.

I. Introduction

The continuing interest in single-wall carbon nanotubes[1,2] (SWNTs) is based on their well-defined structure, stability, and many interesting properties linked to their small diameter and large aspect ratio.[3] SWNTs usually exist as bundled structures held together by a combination of van der Waals and very weak covalent interactions.[4] Since the most intriguing applications in nanoelectronics and structural materials require isolated SWNTs,[5] the development of efficient methods to debundle and disperse SWNTs is highly desirable. Techniques to disperse SWNTs include physical agitation using ultrasonic waves and the addition of chemical surfactants or polymers. Ultrasonic cavitation is known to be destructive and can shorten SWNTs.[6,7] Cavitation is also reported to induce undesired chemical reactions between SWNTs and dispersing solvents like *ortho*-dichlorobenzene.[8] Surfactant or polymer additives coat SWNT surfaces and thus effectively reduce inter-tube attraction. They do not however penetrate deep into rigid nanotube bundles limiting their ability to disperse high concentrations of SWNTs.

Chemical functionalization of SWNTs has emerged as a powerful, alternative approach to disperse SWNTs. The well-studied oxidation of SWNTs using some combination of sulfuric acid, nitric acid, and occasionally hydrogen peroxide[9,10] has been demonstrated to result in better dispersions of SWNTs in aqueous solution, consistent with the addition of polar, hydrogen-bonding functional groups. This harsh treatment is known to open SWNT endcaps, shorten tube lengths, and leave carboxylic acid functional groups at dangling carbon atom sites.

Other chemical functionalization strategies improve SWNT dispersion in less destructive manners. These include azomethine ylide addition,[11] aryl diazonium addition,[12] and fluorination.[13,14] These chemistries largely impact the sidewalls of the SWNTs

† Department of Chemistry and Materials Science Program, University of New Hampshire.
‡ Department of Physics and Astronomy, University of Nevada Las Vegas.
§ Department of Chemistry, University of Nevada Las Vegas.
|| Physics and Astronomy Department, Michigan State University.

(1) Iijima, S.; Ichihashi, T. *Nature* **1993**, *363*, 603.
(2) Bethune, D.; Kiang, C.; de Vries, M.; Gorman, G.; Savoy, R.; Vazquez, J.; Beyers, R. *Nature* **1993**, *363*, 605.
(3) Saito, R.; Dresselhaus, G.; Dresselhaus, M. S. *Physical Properties of Carbon Nanotubes*; Imperial College Press: London, 1998.
(4) Thess, A.; Lee, R.; Nikolaev, P.; Dai, H.; Petit, P.; Robert, J.; Xu, C.; Lee, Y.; Kim, S.; Colbert, D.; Scuseria, G.; Tománek, D.; Fischer, J.; Smalley, R. *Science* **1996**, *273*, 483.
(5) Jorio, A.; Dresselhaus, M.; Dresselhaus, G. *Carbon Nanotubes*: *Advanced Topics in the Synthesis, Structure, Properties and Applications, Topics in Applied Physics*, *Vol. 111*; Springer: New York, 2008.
(6) Lu, K. L.; Lago, R. M.; Chen, Y. K.; Green, M. L. H.; Harris, P. J. F.; Tsang, S. C. *Carbon* **1996**, *34*, 814.
(7) Koshio, A.; Yudasaka, M.; Iijima, S. *Chem. Phys. Lett.* **2001**, *341*, 461.
(8) Niyogi, S.; Hamon, M. A.; Perea, D. E.; Kang, C. B.; Zhao, B.; Pal, S. K.; Wyant, A. E.; Itkis, M. E.; Haddon, R. C. *J. Phys. Chem. B* **2003**, *107*, 8799.
(9) Kuznetsova, A.; Popova, I.; Yates, J. T. J.; Bronikowski, M. J.; Huffman, C. B.; Liu, J.; Smalley, R. E.; Hwu, H. H.; Chen, J. G. *J. Am. Chem. Soc.* **2001**, *123*, 10699.
(10) Wang, Y.; Iqbal, Z.; Mitra, S. *J. Am. Chem. Soc.* **2006**, *128*, 95.
(11) Georgakilas, V.; Voulgaris, D.; Vazquez, E.; Prato, M.; Guldi, D. M.; Kukovecz, A.; Kuzmany, H. *J. Am. Chem. Soc.* **2002**, *124*, 14318.
(12) Stephenson, J. J.; Hudson, J. L.; Leonard, A. D.; Price, B. K.; Tour, J. M. *Chem. Mat.* **2007**, *19*, 3491.
(13) Mickelson, E. T.; Huffman, C. B.; Rinzler, A. G.; Smalley, R. E.; Hauge, R. H.; Margrave, J. L. *Chem. Phys. Lett.* **1998**, *296*, 188.
(14) Khabashesku, V. N.; Billups, W. E.; Margrave, J. L. *Acc. Chem. Res.* **2002**, *35*, 1087.

10.1021/ja0775366 CCC: $40.75

with each addition converting an sp^2 C into an sp^3 C. The addends disrupt intertube van der Waals interactions leading to enhanced dispersions.

Here, we describe a new chemical functionalization strategy that utilizes high boiling polyamines as hydrogenation reagent. The polyamine based hydrogenation of SWNTs is both efficient and thermally reversible. Polyamine hydrogenated SWNTs (H-SWNTs) disperse well in common organic solvents like methanol, ethanol, chloroform, and benzene. Spectroscopic evidence combined with *ab initio* calculations confirms hydrogen chemisorption on the nanotube walls. Theoretical results characterize the nature of the adsorption bond, identify the preferential adsorption geometries at different coverages, and provide quantitative predictions for the effect of hydrogen on the inter-tube distances and interaction energies. Electron microscopy observations, in accord with calculations, indicate that H-SWNTs are weakened structures with significant surface modifications and reduced inter-tube attractions.

II. Experimental Section

SWNTs with stated purities in excess of 90% were purchased from Cheap Tubes, Inc. Several commercially available high boiling polyamines were successfully utilized as SWNT hydrogenation reagents. They include diethylenetriamine (DET, bp 206 °C), triethylenetetramine (TET, bp 266−7 °C), tetraethylenepentamine (TEP, bp 340 °C) and pentaethylenehexamine (PEH, bp 380 °C). For all but PEH, hydrogenation of SWNTs requires operating at temperatures above the boiling point of the corresponding polyamine. Elemental Co (Sigma-Aldrich) with a particle size less than 2 μm is subjected to ball milling (Retsch Mixer Mill 200) at 30 Hz for 100 min to produce Co particles with an average diameter of less than 1 μm. The ball-milled Co is added directly to the polyamine solutions prior to reaction. In a typical polyamine hydrogenation reaction, 5−10 mL of polyamine containing 10 mg Co is utilized for every 100 mg of SWNT. The SWNTs and polyamine are placed in a stainless steel vessel that is sealed and heated to 500 °C for 16−24 h. After cooling, the vessel is opened (CAUTION: pressure release−this operation should be completed in a vented fume hood), ethanol is added, the reaction mixture is filtered, and the solids are washed with copious ethanol to remove polyamine and associated byproducts. The remaining crude reaction mixture is dried under vacuum and characterized.

The morphologies of SWNTs before and after polyamine hydrogenation were compared using a Zeiss/LEO 922 Omega Transmission Electron Microscope (TEM) with accelerating voltages of 120 kV and 200 kV. TEM samples were prepared by placing dispersions on either holey carbon or holey silicon grids and then evaporating the solvent. Raman spectra of H-SWNTs were acquired using a RamanRxn1 Microprobe analyzer (Confocal Raman Microscope, Kaiser Optical Systems). Infrared spectra of H-SWNTs were acquired using a Thermo-Nicolet 6700 FT−IR spectrometer. Fluorolube mulls were prepared by mixing nanotubes and fluorolube oil using a mortar and pestle. The resulting mull was placed between two NaCl plates and the plates pressed together prior to recording the first IR spectrum. Using an iterative process, the film between the NaCl plates was systematically thinned by removing mull from the plates and re-recording until IR spectra of suitable quality were obtained.

III. Computational Methods

To gain fundamental insight into the polyamine hydrogenation process, we studied the hydrogenation reaction, the interaction of hydrogen with carbon nanotubes, and the effect of hydrogen on the nanotube morphology and inter-tube interactions using *ab initio* density functional calculations. Our geometry optimization and total energy calculations are based on the density functional theory (DFT) within the local density approximation (LDA), utilizing first-principles pseudopotentials, as implemented in the DMol3[15] and SIESTA[16] software.

In our DMol3[15] calculations of the interaction of hydrogen with graphene, we used the parametrization of Perdew and Wang[17] for the exchange-correlation energy and a double numerical basis set, including polarization functions on all atoms (DNP). The DNP basis set corresponds to a double-ζ quality basis set with a *p*-type polarization function added to hydrogen and *d*-type polarization functions added to heavier atoms, and is comparable to 6-31G** Gaussian basis sets,[18] providing better accuracy at a similar basis set size.[15,19] In the generation of the numerical basis sets, we used a global orbital cutoff of 3.7 Å. The energy tolerance in the self-consistent field calculations was set to 3×10^{-5} eV. Optimized geometries were obtained without symmetry constraints, using an energy convergence tolerance of 3×10^{-4} eV and a gradient convergence of 5×10^{-2} eV/Å.

In our SIESTA[16] calculations of the structural evolution of hydrogenated single wall carbon nanotubes, we used an optimized double-ζ basis set with polarization orbitals,[20] the Perdew−Zunger[21] parametrization of the exchange-correlation functional, and norm-conserving *ab initio* pseudopotentials[22] in their fully separable form.[23] We used 10^{-2} eV/Å as a strict gradient convergence criterion when determining optimum adsorption geometries.

In order to investigate the interaction of hydrogen with sp^2-hybridized carbon nanostructures, we compared results for narrow single-wall nanotubes to those for graphene, representing the large-diameter limit for nanotubes. The graphene studies were performed for two graphene monolayers with Bernal stacking. In agreement with experimental data, we found the lattice parameter of the relaxed hexagonal primitive unit cell to be $a = 2.45$ Å, corresponding to a C−C bond length of 1.42 Å. Our calculations were performed using $3 \times 3 \times 1$ supercells, separated by $c = 10.00$ Å along the *z* direction. The Brillouin zone was sampled using a $4 \times 4 \times 1$ *k*−point mesh for structural optimizations. Our nanotube studies were performed for (6,6) armchair nanotubes. To represent adequately isolated chemisorbed hydrogen atoms on the (6,6) nanotube in a supercell geometry, we used large unit cells consisting of 6 primitive unit cells and containing 144 C atoms.

For the sake of comparison with FT−IR data, we also calculated the normal modes of model hydrogenated carbon nanostructures. Starting from the relaxed geometry of a given model structure, we constructed the Hessian matrix using finite differences of the analytic gradient of the energy with respect to the atomic positions. The Hessian was evaluated using a 2-point difference of analytic forces, the finite differenciation proceeding from atom to atom. The vibrational frequencies were obtained by matrix diagonalization of the resulting Hessian matrix in mass-weighted Cartesian coordinates. In turn, diagonalization of the Cartesian matrix yielded the vibrational normal modes.

IV. Results and Discussion

A. Experimental Evidence of SWNT Hydrogenation and De-bundling. The chemistry underlying the polyamine hydrogenation process evolved from our successful polyamine hydrogenation of other nanostructured carbons, namely [60]-fullerene,[24] [70]fullerene, and large fullerenes up to and includ-

(15) Delley, B. *J. Chem. Phys*. **1990**, *92*, 508.
(16) Soler, J. M.; Artacho, E.; Gale, J. D.; García, A.; Junquera, J.; Ordejón, P.; Sánchez-Portal, D. *J. Phys: Cond. Mat*. **2002**, *14*, 2745.
(17) Wang, Y.; Perdew, J. P. *Phys. Rev. B* **1992**, *45*, 13244.
(18) Hehre, W. J.; Radom, L.; Schleyer, P. R.; Pople, J. A. *Ab Initio Molecular Orbital Theory*; Wiley: New York, 1986.
(19) Delley, B. *Phys. Rev. B* **2002**, *65*, 085403.
(20) Junquera, J.; Paz, O.; Sánchez-Portal, D.; Artacho, E. *Phys. Rev. B* **2001**, *64*, 235111.
(21) Perdew, J. P.; Zunger, A. *Phys. Rev. B* **1981**, *23*, 5048.
(22) Troullier, N.; Martins, J. L. *Phys. Rev. B* **1991**, *43*, 1993.
(23) Kleinman, L.; Bylander, D. M. *Phys. Rev. Lett.* **1982**, *48*, 1425.
(24) Briggs, J. B.; Montgomery, M.; Silva, L. L.; Miller, G. P. *Org. Lett.* **2005**, *7*, 5553.

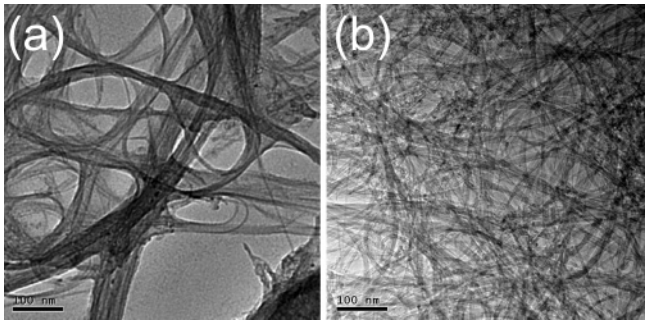

Figure 1. Transmission Electron Microscope (TEM) images of (a) bundled SWNTs before hydrogenation and (b) debundled H-SWNTs after polyamine hydrogenation.

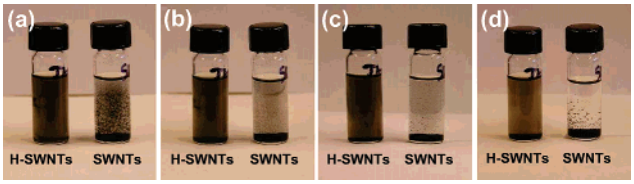

Figure 2. Visual comparison of SWNT and H-SWNT suspensions in methanol for variable times after 30 s of low-power sonication. Time since sonication is 30 s (a); 5 min (b); 1 h (c); and 48 h (d).

ing [250]fullerene.[25] Previous approaches to hydrogenate SWNTs have utilized dissolving metal reductions,[26] high presssure hydrogenations,[27,28] or H-plasma procedures.[29−31] We consider the polyamine hydrogenation process to be superior to other hydrogenations because it is simple, high yielding, easy to workup and scalable.

Because SWNTs are less reactive than fullerenes, we have utilized relatively high reaction temperatures and elemental cobalt as catalyst. Similar conditions have also been employed to hydrogenate fullerenes.[25] For both fullerenes and SWNTs, we observe only hydrogenation, and do not observe alkylation or amination, or any other byproducts.

TEM images recorded before and after polyamine hydrogenation of SWNTs reveal striking differences. Before hydrogenation, the pristine SWNTs are largely bundled, as expected. After polyamine hydrogenation, the H-SWNTs appear as highly dispersed solids on the TEM grid as shown in Figure 1. These observations are corroborated by attempts to disperse SWNTs and H-SWNTs in organic solvents. After 30 s of low-power sonication in methanol, pristine SWNTs quickly fall out of solution, as illustrated in Figure 2. By contrast, H-SWNTs stay well dispersed for days. H-SWNTs also stay well dispersed for days or longer in a variety of other common organic solvents including ethanol, chloroform, and benzene.

Electron microscope images of H-SWNTs, shown in Figure 3, reveal significant surface modification as a result of polyamine

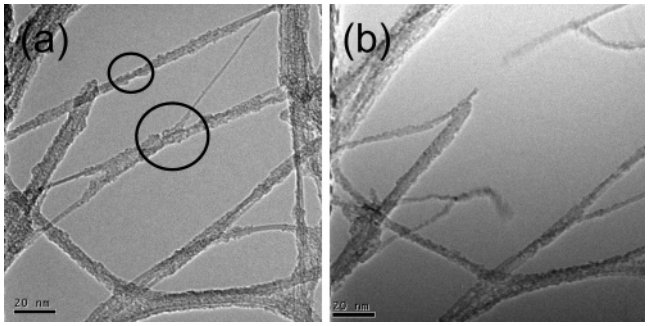

Figure 3. Time sequence of Transmission Electron Microscope images of de-bundled H-SWNTs after polyamine hydrogenation. Hydrogen-induced destabilization makes nanotubes prone to fracture, as seen by changes in the circled areas of (a).

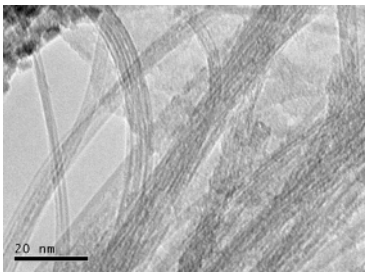

Figure 4. Transmission Electron Microscope image of the initially hydrogenated H-SWNT system of Figure 1(b) following dehydrogenation by annealing at 800 °C.

hydrogenation. The hydrogenated nanotubes are weakened structures that are prone to fracture during irradiation. Thermal gravimetric analysis (TGA) under an inert gas atmosphere indicates an 8% weight loss from room temperature to 800 °C. Pekker and co-workers reported qualitatively similar TGA data for SWNTs hydrogenated using a dissolving metal reduction,[32] but they observed less than 5% weight loss up to 900 °C, indicating overall lower levels of hydrogenation. In Pekker's work, the effluent gases were analyzed by a mass spectrometer revealing the release of several molecules including hydrogen, methane, and methanol. Thus, also for our H-SWNTs, the H:C ratio cannot be determined based upon TGA analysis alone. However, given the qualitative similarities between the TGA curves, we expect at least 1 H atom for every 10 C atoms on the polyamine hydrogenated SWNTs.

TEM analysis of the residual tubes after thermal annealing to 800 °C provides evidence for the reversible nature of hydrogenation. After annealing, as seen in Figure 4, the sample structure strongly resembles that of pristine SWNTs before hydrogenation.

Our Raman characterization of the H-SWNTs is consistent with the formation of functionalized SWNTs, in which sp^2 carbons are converted to sp^3 carbons. As seen in the Raman spectra depicted in Figure 5, the D band, indicative of sp^3 carbon formation along the sidewalls of the SWNT and centered at approximately 1300 cm^{-1}, grows relative to the graphitic G band, centered at approximately 1580 cm^{-1}, following the hydrogenation.

To further characterize the nature of the bonding to SWNTs, we observed vibrational spectra of H-SWNTs using infrared spectroscopy. Our FT−IR spectra reveal C(sp^3)-H stretching

(25) Kintigh, J.; Briggs, J. B.; Letourneau, K.; Miller, G. P. *J. Mater. Chem.* **2007**, *17*, 4647−4651.
(26) Borondics, F.; Jakab, E.; Pekker, S. *J. Nanosci. Nanotech.* **2007**, *7*, 1551.
(27) Meletov, K. P.; Maksimov, A. A.; Tartakovskii, I. I.; Bashkin, I. O.; Shestakov, V. V.; Krestinin, A. V.; Shulga, Y. M.; Andrikopoulos, K. S.; Arvanitidis, J.; Christofilos, D.; Kourouklis, G. A. *Chem. Phys. Lett.* **2007**, *433*, 335.
(28) Bazhenov, A. V.; Fursova, T. N.; Bashkin, I. O.; Antonov, V. E.; Kondrat'eva, I. V.; Krestinin, A. V.; Shul'ga, Y. M. *Fuller. Nanotub. Carbon Nanostruct.* **2006**, *14*, 165.
(29) Khare, B. N.; Meyyappan, M.; Kralj, J.; Wilhite, P.; Sisay, M.; Imanaka, H.; Koehne, J.; Bauschlicher, C. W., Jr. *J. Appl. Phys. Lett.* **2002**, *81*, 5237.
(30) Khare, B. N.; Meyyappan, M.; Cassell, A. M.; Nguyen, C. V.; Han, J. *Nano Lett.* **2002**, *2*, 73.
(31) Zheng, G.; Li, Q.; Jiang, K.; Zhang, X.; Chen, J.; Ren, Z.; Fan, S. *Nano Lett.* **2007**, *7*, 1622.
(32) Pekker, S.; Salvetat, J.-P.; Jakab, E.; Bonard, J.-M.; Forro, L. *J. Phys. Chem. B* **2001**, *105*, 7938−7943.

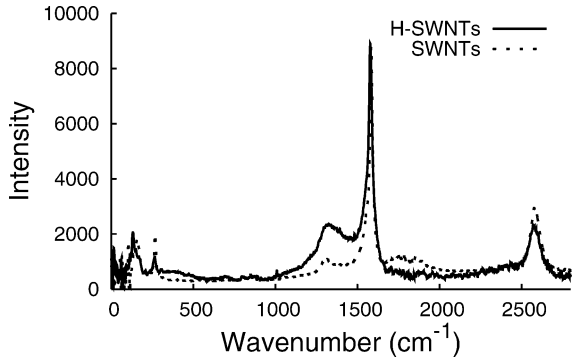

Figure 5. Raman spectra of pristine (SWNTs; dotted line) and hydrogenated (H-SWNTs; solid line) single-wall carbon nanotubes.

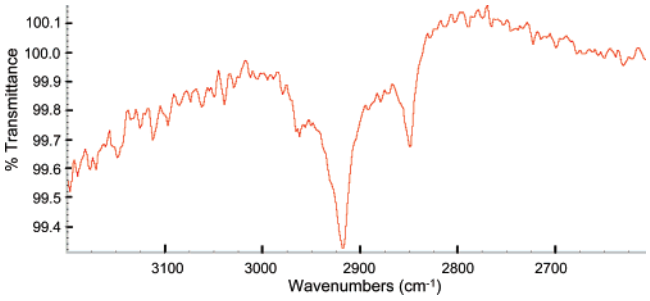

Figure 6. Infrared spectra of hydrogenated nanotubes.

vibrations at 2962 cm^{-1}, 2918 cm^{-1}, and 2849 cm^{-1} as illustrated in Figure 6. Additional IR bands include a relatively intense band at 1580 cm^{-1} corresponding to C═C double bond stretching. Our experimental values for C(sp^3)-H stretching vibrations are in close agreement with those recorded for SWNTs hydrogenated using a H plasma[29] (2955 cm^{-1}, 2924 cm^{-1}, and 2854 cm^{-1}).

B. Theoretical Results for the Interaction of Hydrogen with sp^2-Bonded Carbon Nanostructures. In order to gain fundamental insight into different aspects of the SWNT hydrogenation reported here, we studied the hydrogenation mechanism and the interaction of hydrogen with sp^2-bonded carbon nanostructures. Using *ab initio* density functional calculations, we investigated the nature of the hydrogen adsorption bond and the effect of hydrogen on the morphology and intrinsic stability of individual nanotubes and graphene. As a relevant counterpart to the experimental observations, we present quantitative results for hydrogen-induced changes of the interaction energies and inter-wall distances in assemblies of SWNTs and graphene layers.

Published theoretical results include studies of the bonding character of isolated H atoms on graphitic carbon[33] and controversial results regarding the preferential arrangement of hydrogen pairs on a graphene layer.[34−36] Other investigations address the relative stability of hydrogen pairs adsorbed on the same or on different sides of a graphene layer,[37] and study

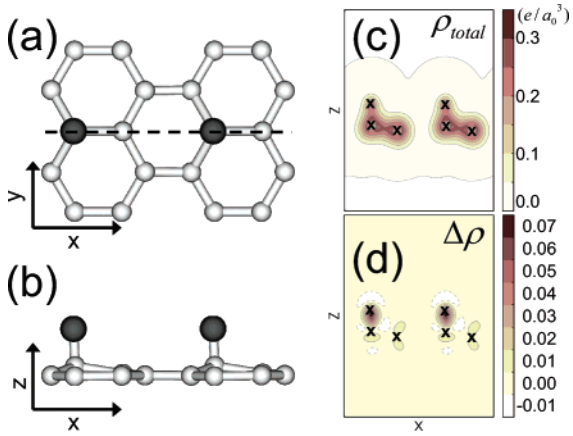

Figure 7. Chemisorption of hydrogen on graphene. Schematic adsorption geometry is shown (a) in top view and (b) in side view, with the cutting plane indicated by the dashed line in (a). Carbon atoms are shown as white, hydrogen atoms as black spheres. (c) Total pseudo-charge density $\rho_{H/graphene}(r)$ and (d) charge density difference $\Delta\rho(r) = \rho_{H/graphene}(r) - \rho_H(r) - \rho_{graphene}(r)$, displayed in the plane used in (b).

graphene with high hydrogen coverage.[38] Theoretical studies of hydrogen-covered nanotubes focused on hydrogen-induced electronic structure changes,[39] the relative stability of different adsorption arrangements,[37,40,41] the possibility of phase-separation into high- and low-coverage regions,[42] and the possibility of axial nanotube cleavage by unzipping in the presence of exohedrally adsorbed H atoms.[41,43]

1. Interaction of Hydrogen with Graphene. We started with the simplest geometry, which involves adsorption of atomic hydrogen on graphene, a good model for a wide-diameter carbon nanotube. Results for the equilibrium adsorption geometry, depicted in Figure 7, parts a and b, suggests that hydrogen preferentially adsorbs on top of carbon atoms at low coverage. In this adsorption geometry, H interacts with the initially unfilled C2p_z orbital on graphene, forming a 1.13 eV strong covalent bond, characteristic of chemisorption. The charge distribution in the H-covered graphene system is depicted in Figure 7c. The nature of the H−C bond can be best seen by inspecting the difference of the total charge density of the system and the charge density associated with the isolated graphene and hydrogen subsystems, shown in Figure 7d. By forming the additional chemisorptive bond, the bonding character of the graphene substrate changes locally from sp^2 to sp^3, thus causing local pyramidalization of the initially planar graphene layer, seen in Figure 7b. The change in bonding character not only makes the hydrogenated surface more reactive, but also destabilizes the graphitic structures, making them more prone to fracture as observed in Figure 3.

At higher coverages, we borrow the terminology used to identify substitutional isomers of benzene, and distinguish pairs of hydrogens adsorbed on adjacent carbon sites, called an ortho arrangement, from pairs of hydrogens on opposite corners of a single C_6 ring, called a para arrangement.[36] In the meta arrangement, hydrogens are neither adjacent nor opposite to each other on a single C_6 ring. The relative stability of these

(33) Jeloaica, L.; Sidis, V. *Chem. Phys. Lett.* **1999**, *300*, 157.
(34) Allouche, A.; Jelea, A.; Marinelli, F.; Ferro, Y. *Phys. Scr. T* **2006**, *124*, 91.
(35) Roman, T.; Diño, W. A.; Nakanishi, H.; Kasai, H.; Sugimoto, T.; Tange, K. *Carbon* **2007**, *45*, 203.
(36) Hornekær, L.; Rauls, E.; Xu, W.; Šljivančanin, Ž.; Otero, R.; Stensgaard, I.; Lægsgaard, E.; Hammer, B.; Besenbacher, F. Phys. *Rev. Lett.* **2006**, *97*, 186102.
(37) Stojkovic, D.; Zhang, P.; Lammert, P. E.; Crespi, V. H. *Phys. Rev. B* **2003**, *68*, 195406.
(38) Allouche, A.; Ferro, Y. *Phys. Rev. B* **2006**, *74*, 235426.
(39) Gülseren, O.; Yildirim, T.; Ciraci, S. *Phys. Rev. B* **2002**, *66*, 121401.
(40) Yildirim, T.; Gülseren, O.; Ciraci, S. *Phys. Rev. B* **2001**, *64*, 075404.
(41) Arellano, J. S.; Molina, L. M.; Rubio, A.; López, M. J.; Alonso, J. A. *J. Chem. Phys.* **2002**, *117*, 2281.
(42) Gülseren, O.; Yildirim, T.; Ciraci, S. *Phys. Rev. B* **2003**, *68*, 115419.
(43) Lu, G.; Scudder, H.; Kioussis, N. *Phys. Rev. B* **2003**, *68*, 205416.

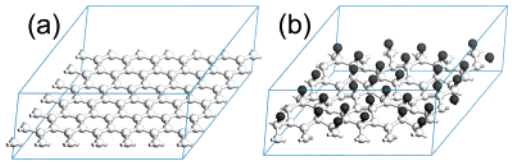

Figure 8. Optimized geometry of (a) pristine graphene and (b) hydrogenated graphene, illustrating the H-induced corrugation of the initially planar layer. Carbon atoms are shown as white, hydrogen atoms as black spheres.

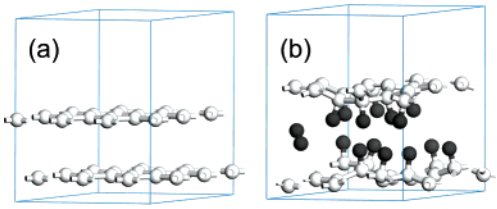

Figure 9. Optimized geometry of (a) a pristine and (b) a hydrogenated graphene bilayer, illustrating a representative arrangement of H atoms, H-induced corrugation and increase of the interlayer distance. Carbon atoms are shown as white, hydrogen atoms as black spheres.

arrangements is a matter of controversy. Whereas the para arrangement has been claimed to be more stable than the ortho arrangement,[36] the opposite stability preference has also been proposed.[34,35] Our results, obtained in large $4 \times 4 \times 1$ supercells, indicate a binding energy for hydrogen of 1.37 eV in ortho and 1.38 eV in para positions, with a negligible energy difference of 0.01 eV. We found that the large adsorption energy differences reported in these arrangements[34−36] were artifacts introduced by the combination of adsorbate-induced stress in the graphene lattice and too small unit cells used in the calculation. Hydrogen binding at meta sites is significantly less favorable.

To study the surface hydrogenation of graphene/graphite, we utilized a H patterning similar to a literature example[34] representing a H/C ratio of 44%, close to the experimental H saturation coverage ranging between 40%[44,45] and 45%.[46] This surface hydrogen adsorption geometry corresponds to a combination of H atoms arranged as contiguous quartets, bonded to a four-atom segment of a C_6 ring. These quartets are surrounded by dimers in second neighbor sites, occupying para or meta (but not ortho) positions.[34] A snapshot of the optimized geometry of a H-covered graphene monolayer in Figure 8b depicts likely arrangements of H atoms and the H-induced corrugation of graphene.

Next, we considered the effect of hydrogen chemisorption on the interlayer interaction in a graphene bi-layer. In Figure 9 we compare the equilibrium geometry of a pristine graphene bilayer to a snapshot of the optimized bilayer geometry in presence of hydrogen. In the H-covered system, depicted in Figure 9b, we observe a tendency of H atoms, chemisorbed on each monolayer, to form an ordered interface. Upon hydrogenation of this model system, the interlayer spacing between the graphene monolayers increased from $d_{iw} = 3.23$ Å in the pristine system to $d_{iw} = 3.93-5.23$ Å. We also found the energy to separate a graphene bilayer to increase from 1.34 eV/nm^2 in the pristine system to 1.68 eV/nm^2 in the hydrogen-covered system. The increased interlayer separation in the hydrogenated system is caused by the pyramidalization at C sites connected to H atoms. The resulting surface corrugation, depicted in Figure 9b, is to some degree analogous to that observed in H-SWNTs, shown in Figure 3.

2. Interaction of Hydrogen with Carbon Nanotubes. Even though graphite serves as a very good model for carbon nanotubes, the effect of hydrogen adsorption on the two systems differs for several reasons. For one, single-wall carbon nanotubes, obtained by rolling up a graphene strip, are intrinsically more rigid and more difficult to deform than graphene monolayers. Also, in contrast to planar graphene, nanotubes are under internal stress. Local weakening of the carbon backbone structure in the vicinity of chemisorbed hydrogen favors stress release associated with significant structural changes. Finally, the local nanotube curvature adds fractional sp^3 character to the dominant sp^2 bonding character especially in narrow SWNTs, making them more reactive.

Once a hydrogen atom is chemisorbed on a nanotube, it may move from one adsorption site to another by overcoming the activation barrier for displacement, which may be lower than the desorption energy. We determined the activation barrier associated with hydrogen diffusion along the nanotube surface by optimizing the adsorption geometry of hydrogen constrained to a plane normal to the nanotube axis. Using a succession of constraining planes, which define the axial position of hydrogen, we obtained a total energy profile. Interpreting this energy profile leads to the interesting result that sigmatropic rearrangement associated with the diffusion of isolated H atoms along the tube surface requires an activation barrier of only ~1 eV, end even less for pairs. Consequently, the hydrogens should be moderately mobile on the nanotube under the experimental reaction conditions, capable of locating the optimum adsorption site.

To identify the preferred adsorption site, we optimized the H adsorption geometry on a (6,6) nanotube for selected low-coverage adsorbate arrangements, shown in Figure 10, and compared their energy. In the following, we will list the calculated hydrogen binding energies on the nanotube per pair of adsorbed hydrogen atoms, with respect to free H_2 molecules, based on DFT total energies of the reference systems.

In the nonplanar geometry of a nanotube, we expect the energetic preference between ortho and para arrangements of hydrogen pairs to differ from our above results for graphene due to differences in the associated level of nanotube stress release. A pair of H atoms prefers to chemisorb on an armchair (6,6) SWNT exohedrally in ortho geometry, bonded to a pair of neighboring carbons aligned along the nanotube axis, as shown in Figure 10a. Also on the zigzag (12,0) nanotube, ortho adsorption of hydrogen pairs along the axis is favored energetically. As an interesting general trend, we thus predict that chemisorbed hydrogens should preferentially form axially aligned chains. An isolated pair of ortho H on a (6,6) SWNT gains 0.15 eV with respect to free H_2. As discussed earlier, H chemisorption causes pyramidalization at the nanotube surface, which in this case translates into a radial outward displacement by 0.46 Å of the underlying C atom.

Even more stable than an isolated pair of ortho adsorbates is a chain of exohedral ortho hydrogens, aligned along the tube axis, schematically shown in Figure 10b. In this geometry, each

(44) Haasz, A. A.; Franzen, P.; Davis, J. W.; Chiu, S.; Pitcher, C. S. *J. Appl. Phys.* **1995**, *77*, 66.
(45) Zecho, T.; Güttler, A.; Küppers, J. *Carbon* **2004**, *42*, 609.
(46) Ugolini, D.; Eitle, J.; Oelhafen, P. *Appl. Phys. A: Solids Surf.* **1992**, *54*, 57.

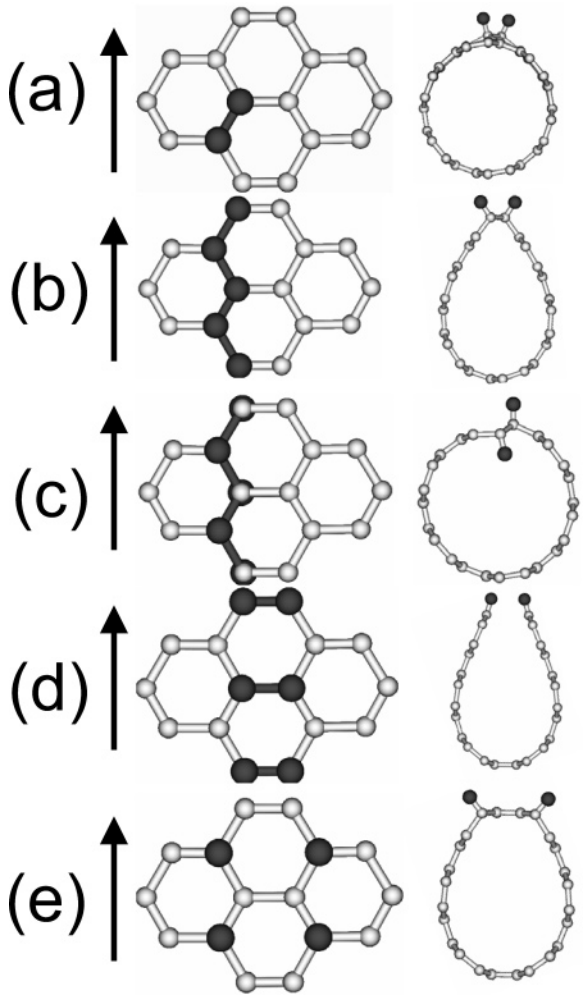

Figure 10. Schematic depiction of possible low-coverage H adsorption geometries on the wall of a (6,6) single-wall carbon nanotube, in side view (left panels) and end-on view (right panels). Carbon atoms are shown as white, hydrogen atoms as larger black spheres. Carbon bonds most affected by the adsorption are emphasized by the black lines. The axis direction is indicated by arrows. Particular geometries are discussed in the text.

pair of H atoms gains the large energy amount of 1.07 eV with respect to free H_2. This is significantly more than for an isolated ortho pair, and also the highest value among the geometries studied here. Much of this extra binding energy comes from an egg-type distortion of the nanotube, caused by the local $sp^2 \rightarrow sp^3$ conversion and reflected in the C−C bond length increase from 1.42 Å to 1.51 Å near the hydrogen chain, depicted in the right panel of Figure 10b. For the sake of comparison, we also considered an alternating exo-/ endohedral chain of ortho hydrogens along the tube axis, shown in Figure 10c. The binding energy of 0.17 eV for a pair of hydrogens is much lower than for the all-exohedral chain, even though the C−C bond length near the hydrogens is the same in both cases. The unfavorable bonding is caused by the additional stress associated with alternating convex/concave distortion at the nanotube surface.

Even though isolated ortho pairs aligned normal to the tube axis are not as stable as those along the axis, this adsorption geometry, depicted in Figure 10d, causes the largest nanotube distortion. Independent of whether the hydrogens are initially chemisorbed exo- or endohedrally, the nanotube unzips axially, without activation barrier, into a horseshoe shape[41,43] shown in the right panel of Figure 10d. The weak interaction between the hydrogenated edges, at relatively large interatomic distances across the gap of $d_{CC} = 2.77$ Å and $d_{HH} = 2.18$ Å near the edges, prevents spontaneous, i.e., activation-free, unravelling to a graphene ribbon. Much of the large energy gain of 0.87 eV per hydrogen pair comes from the structural relaxation and the energy gain associated with the decoration of edges by the hydrogens. In comparison to the chain of ortho pairs in Figure 10d, the energy gain associated with forming a chain of para pairs normal to the axis, depicted in Figure 10e, is very small at 0.07 eV per hydrogen pair.

To decide whether hydrogen adsorption in chains along the perimeter is more favorable than forming infinite chains along the axis, we compared the binding energies in these two arrangements. We found chemisorbed ortho hydrogens forming a symmetric ring of six pairs along the perimeter to be very unstable. Three pairs of chemisorbed para hydrogens, forming a symmetric ring along the perimeter, are more favorable, but still less stable by 0.03 eV than three free H_2 molecules. Our calculations suggest that bonding along the perimeter is more favorable and becomes eventually exothermic if only a small fraction of the ring is occupied densely, thus causing deformation and breaking the symmetry by releasing stress. For any adsorption geometry studied, the energy gain associated with forming a partly filled ring along the perimeter was much smaller than the 1.07 eV value for an infinite line of ortho hydrogens along the nanotube axis.

For hydrogen adsorption on nanotubes at higher coverages, we base our geometry selection on the fact that the most stable adsorption arrangement involves lines of hydrogens along the axis. Since additional hydrogen chains may help to further release the stress in the nanotube structure, we expect hydrogen adsorption in such arrangements to be still more energetically favorable. In what turns out to be the most stable arrangement, two axially aligned chains of exohedral ortho hydrogens are adsorbed on opposite sides of the nanotube, as shown in Figure 11a. Stress release due to local rebonding near the hydrogen chains contributes significantly to the high binding energy of 1.39 eV per hydrogen pair. The resulting flattened structure, clearly seen in the right panel of Figure 11a, is a precursor to forming a bi-ribbon with Klein-edges terminated by C−H radicals. In contrast to this result, adjacent exohedral ortho hydrogen chains are very unstable energetically. Corresponding exohedral second-neighbor chains, depicted in Figure 11b, are more stable, yielding an energy gain of 0.68 eV per hydrogen pair.

Finally, we compared our results for zigzag chains of hydrogens in Figure 11, parts a and b, to those for axially aligned chains of exohedral ortho hydrogens that are paired normal to the axis, as shown in Figure 11c. We considered two of these hydrogen chains adsorbed on opposite sides of the nanotube. Even though the ortho adsorption geometry normal to the axis is less stable than the axial zigzag arrangement, this particular bonding allows an activation-free transition to a pair of graphene ribbons with H-terminated zigzag edges. An even larger nanotube relaxation energy than in the geometry of Figure 11a contributes to the large hydrogen binding energy of 1.59 eV per hydrogen pair. This and other large structural changes, predicted in our calculations, are caused by hydrogen-induced destabilization of the sp^2 bonded carbon nanostructures. This

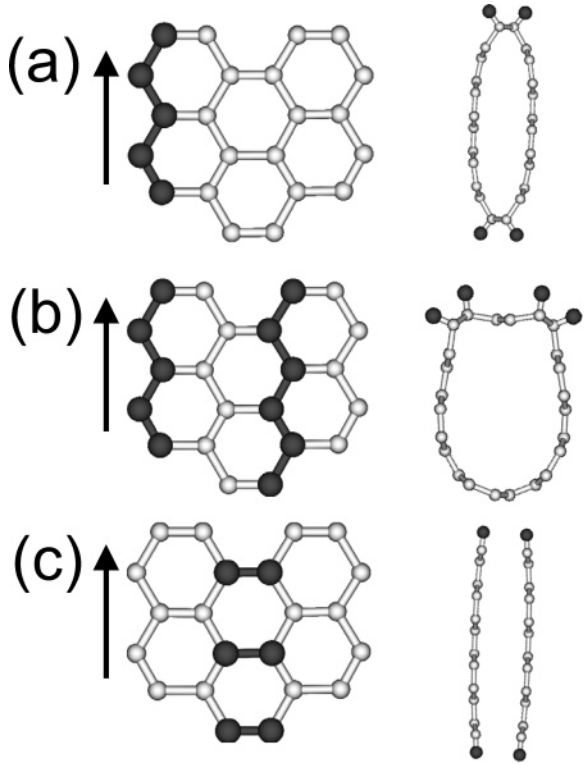

Figure 11. Schematic depiction of possible high-coverage H adsorption geometries on the wall of a (6,6) single-wall carbon nanotube, in side view (left panels) and end-on view (right panels). Carbon atoms are shown as white, hydrogen atoms as larger black spheres. Carbon bonds most affected by the adsorption are emphasized by the black lines. The axis direction is indicated by arrows. Particular geometries are discussed in the text.

can be viewed as the underlying cause of the hydrogen-induced embrittlement, observed in the electron micrographs of hydrogenated nanotubes in Figure 3.

As discussed earlier, hydrogen adsorption increases the interlayer distance and separation energy in graphene bilayers, shown in Figure 9. We observe a very similar trend with SWNTs when comparing the interaction between pristine or hydrogen-covered (6,6) SWNTs for either a pair or an infinite triangular lattice nanotubes. Since interlayer interactions and optimum energies of pristine and hydrogenated nanotubes are known to depend sensitively on the choice of the basis, we checked the convergence of our DFT results using a localized basis to plane-wave calculations for the infinite lattice.

We consider a monolayer coverage in our calculations, corresponding to one H atom per carbon in the nanotube. At this coverage, the diameter of a (6,6) nanotube increases by 15% from 0.82 nm in the pristine system to 0.94 nm in the H-covered system. Exposure to hydrogen also causes a 6% axial expansion. The effect of hydrogen adsorption on the equilibrium geometry of a nanotube pair can be seen in Figure 12. The presence of chemisorbed hydrogen not only causes an increase in the nanotube diameter, but also maximizes the inter-tube contact area by flattening the softer hydrogenated nanotube in the contact area, as seen clearly in Figure 12b. These deformations are suppressed in nanotube bundles by the imposed sixfold symmetry of the triangular lattice. In the infinite bundle, the inter-wall distance increases by 11% from $d_{iw} = 3.13$ Å in the pristine system to $d_{iw} = 3.50$ Å in the H-covered system. The energy gain per nanotube, associated with the formation of a triangular lattice, increases from 1.16 eV/nm in the pristine

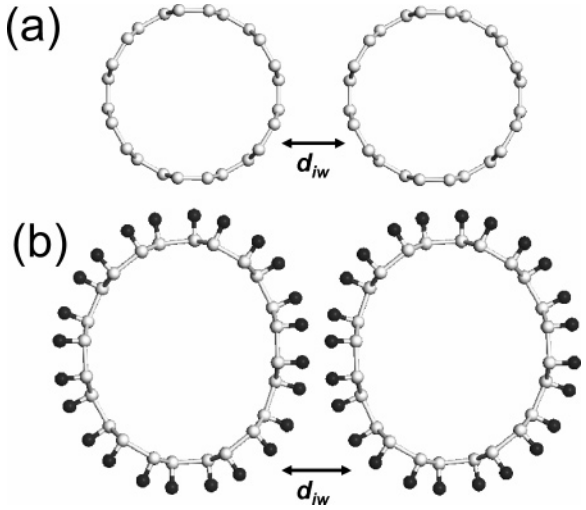

Figure 12. Optimized geometry of a pair of (a) pristine and (b) hydrogenated (6,6) single-wall carbon nanotubes. Carbon atoms are shown as white, hydrogen atoms as larger black spheres. d_{iw} refers to the inter-wall distance.

system to 3.25 eV/nm in the hydrogenated system. Assuming pairwise inter-tube bonds in the infinite lattice, this translates into the separation energy $E_{sep} = 0.39$ eV/nm for a pristine and $E_{sep} = 1.08$ eV/nm for a hydrogenated nanotube pair.

One of our intriguing results is the predicted increase in the separation energy of graphene and nanotubes when covered by hydrogen. For the sake of computational convenience, we studied artificially high hydrogen coverages of graphene and nanotubes. At these high coverages, the hydrogenated system is often only metastable with respect to the pristine system and free H_2 molecules. As two hydrogenated surfaces are brought to close vicinity, a large number of hydrogen atoms becomes confined in the restricted inter-wall space. Initially chemisorbed hydrogens on the confining nanotube/graphene walls start interacting with a tendency to form H_2 molecules, albeit subject to unrealistically high gas pressures that impose an energy penalty. The chemisorbed hydrogen is thus frustrated by its inability to desorb and form H_2 gas according to its initial energetic preference because of the energy penalty to do so in the restricted inter-wall space. The calculated enhancement of the energy to separate hydrogenated graphene and nanotubes thus only reflects the covalent H−H interaction in the frustrated state associated with large hydrogen coverages. At lower hydrogen coverages, the separation energy is likely to decrease.

At first glance, our finding of a stronger interaction between hydrogenated nanotubes and graphene bilayers contradicts the observed de-bundling effect attributed to hydrogenation. To understand de-bundling in the real system, however, we must consider the presence of polyamine hydrogenating agents and the solvent. We should expect de-bundling to be initiated by residual polyamines, which also act as surfactants. Additional de-bundling should occur in the presence of the solvent, which can penetrate more easily inside hydrogenated bundles that exhibit a larger inter-tube spacing. Solvents are likely to react more strongly with H-SWNTs due to their partial sp^3 bonding character, thus causing the observed de-bundling.

For the sake of comparison with the vibrational spectra in Figure 6, and as a further characteristic of the bonding character, we also calculated the vibrational modes of hydrogen adsorbed on graphitic carbon. We considered a model system containing

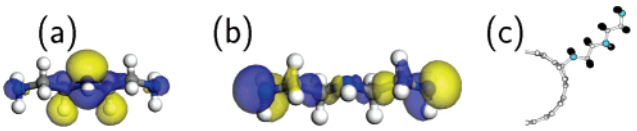

Figure 13. Equilibrium structure superimposed with (a) the highest occupied molecular orbital (HOMO) and (b) the second highest occupied molecular orbital (HOMO-1) of the polyamine molecule diethylenetriamine (DET). (c) Likely docking geometry of DET on the (6,6) carbon nanotube, where hydrogen transfer from the amine radical to the nanotube is most likely to occur.

either a single H atom or ortho and para hydrogen pairs adsorbed on a graphene monolayer and calculated the normal modes of the C(sp^3)-H stretching vibrations. Since the nature and stability of the C−H bond on graphene and nanotubes is very similar, and since vibrational spectra are determined by the force constants and the atomic masses only, we expect the C−H related vibrational spectra on graphene and nanotubes to be essentially the same. The calculated C−H stretching frequency for a single H atom adsorbed on a graphene monolayer is 2689 cm^{-1}. The added stability resulting from ortho and para pairing of hydrogens, discussed above, blue-shifts this frequency to 2878 cm^{-1} and 2853 cm^{-1} for ortho pairs (symmetric and asymmetric C(sp^3)-H stretching, respectively), and to 2742 cm^{-1} and 2765 cm^{-1} for para pairs. The experimentally observed C(sp^3)-H stretching vibrations for H-SWNTs in the range 2849 − 2962 cm^{-1} suggest that polyamine hydrogenation occurs preferentially with the more stable ortho hydrogen pairing.

3. Mechanism of Polyamine Hydrogenation. The recently proposed hydrogenation mechanism of [60]fullerene by polyamines[25] involves an electron transfer from the polyamine to the fullerene, followed by a proton transfer from the N−H group to [60]fullerene, resulting in a neutral $C_{60}H$ radical and a neutral N-centered polyamine radical that is missing one hydrogen. The electron transfer is believed to involve the pronounced charge density lobe near the N atom in the nonbonding HOMO and HOMO-1 orbitals of the polyamine molecule diethylenetriamine (DET), depicted in Figure 13, parts a and b.

In the case of diethylenetriamine reacting with a nanotube, the total energy of the system after one hydrogen transfer, yielding a hydrogenated nanotube radical and an isolated neutral DET radical, has risen by 3.6 eV. Since the hydrogen transfer between isolated entities is thermodynamically unfavorable, the mechanism likely involves diethylenetriamine chemisorption on the nanotube as a necessary step.[47] The likely adsorption geometry of DET on the (6,6) nanotube is depicted in Figure 13c. In this docking arrangement, the charge density lobes of the HOMO and HOMO-1 orbitals near the N sites are overlapping with the unfilled C2$p_\perp$ states on the nanotube, thus reducing the energy barrier for hydrogen transfer.[47]

V. Summary and Conclusions

In conclusion, we combined experimental observations with *ab initio* calculations to study the reversible hydrogenation of single-wall carbon nanotubes (SWNTs) using high boiling polyamines as hydrogenation reagents. Our calculations characterize the nature of the adsorption bond and identify preferential adsorption geometries at different coverages. Theoretical results, combined with transmission electron microscopy, Raman spectroscopy, infrared spectroscopy, and thermal gravimetric analysis data lead us to conclude that chemisorbed hydrogen modifies the structure and stability of nanotubes significantly and increases the inter-tube distance, thus explaining the improved dispersability of H-SWNTs in solvents like methanol, ethanol, chloroform, and benzene.

Acknowledgment. We acknowledge useful discussions with Hua Jiang. G.M., J.K., D.T. and S.B. acknowledge financial support from the Nanoscale Science and Engineering Center for High-rate Nanomanufacturing (NSF NSEC Grant No. 425826). D.T. and S.B. also acknowledge additional support from the National Science Foundation (NSF-NIRT Grant No. ECS-0506309). P.W. and E.K. acknowledge support from the U.S. Department of Energy (DOE grant No. DE-FG36-05GO-85028). Computational resources have been provided by the Michigan State University High Performance Computing Center.

JA0775366

(47) Kim, E.; Weck, P. F.; Miller, G. P.; Berber, S.; Tománek, D., in preparation.